

Search for age pattern across spiral arms of the Milky Way

Zhi-Hong He (何治宏)^{1,2}, Ye Xu (徐烨)¹ and Li-Gang Hou (侯立刚)^{3,4}

¹ Purple Mountain Observatory, Chinese Academy of Sciences, Nanjing 210023, China

² University of Science and Technology of China, Hefei 230026, China

³ National Astronomical Observatories, Chinese Academy of Sciences, Beijing 100101, China

⁴ CAS Key Laboratory of FAST, National Astronomical Observatories, Chinese Academy of Sciences, Beijing 100101, China

Received 2020 July 16; accepted 2020 September 1

Abstract The age pattern across spiral arms is one of the key observational features utilised to study the dynamic nature of the Galaxy's spiral structure. With the most updated samples of high-mass star formation region (HMSFR) masers, O stars and open clusters, we investigated their distributions and kinematic properties in the vicinity of the Sun. We found that the Sagittarius-Carina Arm traced by HMSFRs, O stars ($\lesssim 10$ Myr) and young open clusters (<30 Myr) seem to deviate gradually towards the Galactic Anticenter (GAC) direction. The Local Arm traced by HMSFRs, O stars, young clusters and also medium-young clusters (30–100 Myr) are inclined to gradually deviate toward the Galactic Center (GC) direction. The properties for the Local Arm are supported by a simplified simulation of cluster motions in the Galaxy. Indications of systematic motions in the circular and radial velocities are noticed for the old open clusters (>200 Myr). These results are consistent with the idea that star formation can be triggered by spiral shocks of density waves, and indicate that the corotation radius of the Galaxy is located between the Sagittarius-Carina Arm and the Local Arm, close to the Solar circle.

Key words: Galaxy: disk — Galaxy: structure — Galaxy: kinematic and dynamics — open clusters and associations: general — Stars: massive

1 INTRODUCTION

In the local Universe, at least 30% of massive galaxies are spiral galaxies (Willett et al. 2013; Ann et al. 2015; Kuminski & Shamir 2016). The formation mechanism of spiral arms, as the typical characteristic of spiral galaxies, is still a matter of debate (e.g., Dobbs & Baba 2014). Several different mechanisms have been proposed to explain the diversity of the observed spiral patterns, e.g., quasi-stationary density wave theory, which suggests that the spiral arms are long-lived, stationary and rigidly rotating (Lindblad 1963; Lin & Shu 1964, 1966; Shu 2016; Peterken et al. 2019), local instabilities, perturbations or noise induced spiral arms, which are transient and recurrent in nature (Goldreich & Tremaine 1978; Toomre 1981; Sellwood & Carlberg 1984; Baba et al. 2009), tidal interactions (e.g., Toomre & Toomre 1972; Dobbs et al. 2010) and bar driven spirals (e.g., Sanders & Huntley 1976; Tagger et al. 1987; Sellwood & Sparke 1988; Athanassoula et al. 2010).

Observational tests have been made toward many face-on spiral galaxies, in order to understand the underlying

dynamics (e.g., Martínez-García et al. 2009; Chandar et al. 2017; Miller et al. 2019). Toward the grand-design spiral galaxy UGC 3825, Peterken et al. (2019) measured the offset between young stars of a known age and the spiral arm where the stars formed, and found a pattern speed which varies little with radius. Their results are consistent with a quasi-stationary density wave. Masters et al. (2019) studied the correlation between the bulge prominence and spiral arm tightness by considering a large sample of galaxies, but at best a weak correlation between them was found, which suggests that the majority of spiral arms may be not static density waves. A similar conclusion was also derived by Hart et al. (2017). Yu & Ho (2018) found that the pitch angle of spiral arms decreases statistically significantly from the reddest to the bluest bandpass for a sample of galaxies, which can be naturally interpreted by density wave theory. Also, Pringle & Dobbs (2019) found that the pitch angle data of Yu & Ho (2018) are consistent with a picture that the pitch angles evolve in time, which indicate that the idea that most spiral structure is generated by tidal interactions and/or by internal self-gravity is still viable. Shabani et al. (2018) found a significant age

gradient across the spiral arms in the grand-design spiral galaxy NGC 1566, which is consistent with the prediction of stationary density wave theory. But for the other two galaxies, M51a and NGC 628, no age gradients across spiral arms were found, which indicate that the spiral structures in these two galaxies are not the result of a stationary density wave. It seems that whether galaxies display quasi-stationary density waves, local instabilities induced spirals, tidally induced spirals or bar driven spirals is still not conclusive (e.g., Dobbs & Baba 2014).

For the Milky Way Galaxy we reside in, both its morphology of spiral structure and the nature of spiral arms have not yet been well determined (e.g., Dobbs & Baba 2014; Xu et al. 2018a). It has long been suggested that the Milky Way is probably a grand design spiral, as large-scale spiral arm segments were traced by, e.g., HII regions, high-mass star formation regions (HMSFRs) and HI gas (Georgelin & Georgelin 1976; Levine et al. 2006; Hou & Han 2014; Reid et al. 2019). However, some recent studies discovered more than one spur and/or branch-like feature in the vicinity of the Sun (Xu et al. 2016, 2018b; Chen et al. 2019), which implied that the Milky Way probably is different from a pure grand design spiral, but seems to resemble multi-armed galaxies (e.g., M101). Some theoretical works also suggested that the observed velocity data of Galactic gas and/or stars can be explained by dynamic rather than stationary spiral arms (e.g., Baba et al. 2009; Baba, Saitoh, & Wada 2010). The grand design or multi-armed nature is linked to the underlying dynamics in the Milky Way, which are expected to be better verified along with the constantly improving quality of observational data.

Different approaches have been applied to understand the nature of Galaxy spiral arms based on observational data. The first one is through the analysis of perturbed stellar velocity distributions in the vicinity of the Sun, which can be induced by spiral structure (Williams et al. 2013; Faure et al. 2014; Liu et al. 2017; Kawata et al. 2018). For instance, by using the LAMOST-*Gaia* common stars, Liu et al. (2017) found that the in-plane velocity fields for nearby young stars are different from those of old stars, which suggest that the young stars are associated with a density wave near the Local Arm. Hunt et al. (2017) found a group of stars which have systematically high rotation velocity outside of the Solar radius, and suggested that a possible cause of this feature is the co-rotation resonance of the Perseus Arm. Griv et al. (2020) analyzed the distances, and radial and azimuthal velocities of a sample of *Gaia* stars in the solar neighbourhood on the assumption of density wave theory. They proposed that the Local Arm is part of a predominant density-wave structure in the Galaxy. Besides spiral arms in the Galactic disk, the central Galactic bar(s), perturbation of a nearby dwarf galaxy or a dark matter sub-halo are also capable of

inducing perturbed velocities (e.g., see Gómez et al. 2013; Bovy et al. 2015; Cheng et al. 2019), which are difficult to distinguish in observations at the moment.

The second method is through comparison of the relative positions of gaseous/dusty arms and stellar arms in the Milky Way (e.g., Hou & Han 2015; Monguió et al. 2015). According to the star formation scenario of density wave theory, gas is compressed by a shock wave caused by stellar arms, leading to the formation of new stars. The latter will move at a different speed than the stellar arms, resulting in systematic position offsets between the gaseous/dusty and old stellar arms (or displayed as clear age pattern or colour gradients in observations, e.g., Roberts 1969; Shu 2016; Dobbs & Pringle 2010; Shabani et al. 2018; Peterken et al. 2019). The direction of the position offsets changes at the corotation radius (R_c) as illustrated in figure 8 of Shu (2016), where the angular speed of the local matter coincides with the pattern speed of spiral arms (e.g., see Puerari & Dottori 1997; Martínez-García et al. 2009; Dias et al. 2019). The pitch angles of Galactic spiral arms traced by gas or recent star formation are expected to be larger than those of old stars. In the case of dynamic spiral arms, the position offsets or age pattern may be also presented, but the distribution of stellar ages is chaotic and the age pattern is not clear (e.g. Dobbs & Pringle 2010; Wada et al. 2011; Grand, Kawata, & Cropper 2012; Dobbs & Baba 2014). For the Milky Way, observational tests for the nature of spiral arms are very limited, and have only been made in a small portion of the entire Galactic disk: 1) the tangential regions of the Scutum Arm, the Centaurus Arm, and the Near 3-kpc Arm, by analysing the arm tangencies with multiwaveleghth data (e.g., Hou & Han 2015); 2) segment of the Perseus Arm in the vicinity of the Sun, by classifying the stellar Perseus Arm and comparing it with the positions of dust lane and gaseous Perseus Arm (Monguió et al. 2015; Vallée 2018); 3) the Local Arm, by identifying the stellar overdensity, and comparing the pitch angles of the Local Arm traced by old stars and HMSFRs (Miyachi et al. 2019). Whether the spatial offsets or age pattern are widespread in the Galaxy is an important feature for understanding the dynamic nature of spiral arms, and more tests based on observations would be necessary.

In the past few years, the detailed spiral structure within about 4–5 kpc of the Sun have been well established by taking advantage of astrometry measurements from very long baseline interferometry (VLBI) and the *Gaia* mission. Up to now, the parallax distances of about 200 HMSFR masers have been derived (Reid et al. 2019). The HMSFR masers are excellent tracers of spiral arms indicated by on-going massive star formation. The *Gaia* mission (Gaia Collaboration et al. 2016, 2018) has provided a large and uniform sample of O stars with accurate stellar astrometry (Xu et al. 2018b). The O stars of *Gaia* are older

than the very young high-mass stars in the HMSFR sample of [Reid et al. \(2019\)](#) from an evolutionary point of view, but still with ages under ~ 10 Myr. Based on data from the *Gaia* Data Release 2 (DR2), the distance accuracies of more than 1800 open clusters (OCs) have been updated, which are the most precise to date ([Cantat-Gaudin et al. 2018](#); [Cantat-Gaudin & Anders 2020](#); [Cantat-Gaudin et al. 2020](#)). An OC is a group of many stars that formed from the same giant molecular cloud and roughly have the same age. Open clusters have a wide range of ages, from a few million years to more than billions of years. These high quality data enable us to inspect the possible position offsets of spiral arms traced by the objects with different ages (or named age pattern, [Dobbs & Pringle 2010](#)), and better understand the dynamic nature of the nearby spiral arm segments.

This work is organised as follows. In Section 2, we introduce the samples of HMSFR masers, O stars and OCs. In Section 3, we report the statistical results about the distributions and kinematic properties of different kinds of spiral tracers. Discussions and conclusions are given in Section 4.

2 DATA

2.1 HMSFR Masers

Up to now, there are approximately 200 very young high-mass stars with trigonometric parallax and proper motion measurements from their associated molecular masers (e.g., CH₃OH 6.7 GHz maser, H₂O 22 GHz maser, [Reid et al. 2019](#)). The measurements are primarily from the Bar and Spiral Structure Legacy (BeSSeL) Survey¹ and the Japanese VLBI Exploration of Radio Astrometry (VERA) project. Eighty-two of them are located within about 5 kpc of the Sun, with $|z| < 0.2$ kpc and parallax uncertainty $< 10\%$. Here, z is the distance of an object to the Galactic plane. The distribution of the 82 HMSFRs accurately indicates segments of the Sagittarius-Carina Arm, the Local Arm and the Perseus Arm in the vicinity of the Sun. The arm parameters fitted by [Reid et al. \(2019\)](#) are adopted in this work to indicate the positions of spiral arms traced by on-going massive star formation. In the longitude range of about 240° to 340°, there is a lack of data for the HMSFRs with parallax measurements, which can be supplemented by those O stars with *Gaia* parallax information ([Xu et al. 2018b](#)).

2.2 O Stars

In this work, we adopt the catalogue of O stars given by [Xu et al. \(2018b\)](#), which is obtained by a cross-match between the O stars listed in [Reed \(2003\)](#) and the *Gaia*

DR2 database ([Gaia Collaboration et al. 2018](#)). In this catalogue, there are 829 O stars with $|z| < 0.2$ kpc; 366 of them have accurately measured *Gaia* parallaxes, i.e. with parallax uncertainty $< 10\%$. In addition, 208 of the 366 O stars have radial velocities from the SIMBAD database², and 171 with velocity errors. The velocity errors are below 5 km s⁻¹ for 58%, and 10 km s⁻¹ for 91% of the 171 O stars.

2.3 Open Clusters

With the method of artificial neural networks, [Cantat-Gaudin et al. \(2020\)](#), hereafter CG20) derived the distance moduli, ages, mean parallaxes and proper motions for 1867 OCs, 1092 of which are known clusters ([Dias et al. 2002](#); [Kharchenko et al. 2013](#)) and rediscovered by utilizing the *Gaia* DR2 ([Cantat-Gaudin et al. 2018](#)); 775 of the 1867 clusters are identified by [Castro-Ginard et al. \(2018, 2019, 2020\)](#), [Cantat-Gaudin et al. \(2018, 2019\)](#) and [Liu & Pang \(2019\)](#). In this work, we focus on the OCs close to the Galactic disk. The objects with $|z| > 0.2$ kpc are excluded as what we did for the HMSFRs and O stars.

It should be mentioned that the main uncertainty for the parallaxes comes from the unknown systematic error (< 0.1 mas) of the *Gaia* DR2 data ([Lindegren et al. 2018](#)), which has a greater impact on distant clusters than nearby ones. For example, at a heliocentric distance of 2 kpc, the maximum distance error caused by the systematic error could reach 400 pc, which will influence part of the Sagittarius-Carina Arm and the Perseus Arm. For the Local Arm, the influence of the unknown systematic error is expected to be small. In order to weaken the influence of the unknown systematic error, we excluded the OCs with a difference between parallax and photometric distances greater than 100 pc.

Finally, 846 OCs with distances, ages and proper motions are reserved, accounting for about half of the catalogued clusters by CG20. Most of them are within 4 kpc of the Sun. Their ages range from 6 Myr to 2 Gyr; 367 of the 846 OCs have radial velocities from the *Gaia* DR2 ([Soubiran et al. 2018](#)), and more than 92% of them have velocity errors σ_{RV} less than 5 km s⁻¹. The median σ_{RV} is 0.7 km s⁻¹. The median proper motion uncertainties are 0.16 mas yr⁻¹ and 0.15 mas yr⁻¹ for the eastward ($\mu_x = \mu_\alpha \cos(\delta)$) and northward directions ($\mu_y = \mu_\delta$), respectively.

3 AGE PATTERN FOR THE NEARBY SPIRAL ARM SEGMENTS

To search for possible position offsets of spiral arms traced by objects with different ages (i.e., the age pattern),

¹ <http://bessel.vlbi-astrometry.org/>

² <http://simbad.u-strasbg.fr/simbad/sim-fcoo>

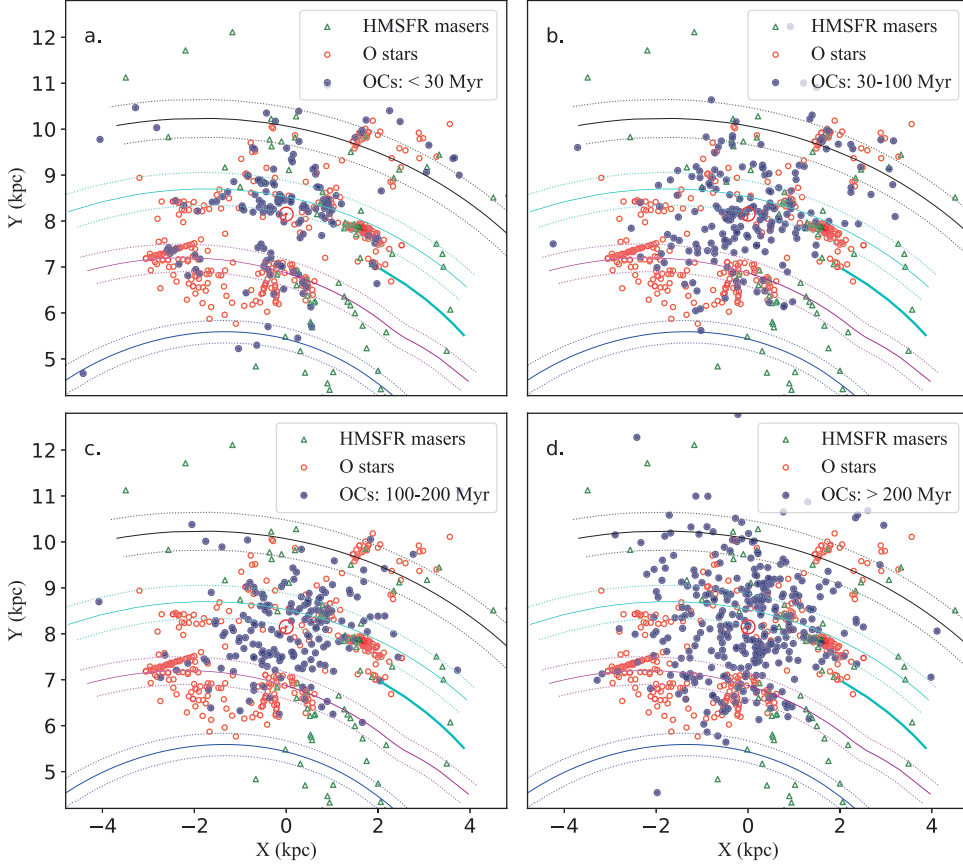


Fig. 1 Projected distributions of OCs for different age groups (*filled blue circles*) in the Galactic disk. The age ranges of OCs are: Panel (a), 0–30 Myr; Panel (b), 30–100 Myr; Panel (c), 100–200 Myr; and Panel (d), > 200 Myr. Also plotted in each panel are the HMSFR masers (*open green triangles*) and O stars (*open red circles*), in order to visualize the spiral arm segments traced by on-going massive star formation. The Sun is at (0 kpc, 8.15 kpc). The *solid* and *dashed lines* signify the best-fitted spiral arms and arm widths by Reid et al. (2019) respectively. The Perseus Arm (*black*), the Local Arm (*cyan*), the Sagittarius-Carina Arm (*magenta*), the Scutum Arm (*blue*) and the Local spur (*bold cyan*) are indicated by different colours.

we analyse the distributions and kinematic properties of HMSFR masers (very young), O stars ($\lesssim 10$ Myr) and OCs (6 Myr–2 Gyr). As the OCs cover a wide range of ages, we divide them into four different age groups: < 30 Myr (including 163 OCs); 30–100 Myr (194 OCs); 100–200 Myr (169 OCs); and > 200 Myr (320 OCs), to ensure that there are quite a few OCs in each group. In this work, the distance of the Sun to the Galactic center (GC) and the disk mid-plane are set to be $R_0 = 8.15$ kpc and $z_0 = 5.5$ pc (Reid et al. 2019), respectively.

3.1 Distributions

The projected distributions of HMSFR masers, O stars and OCs with different age groups in the Galactic plane are depicted in Figure 1. As a reference, we also plot the best-fitted model of spiral arms derived by Reid et al. (2019) from their trigonometric parallax data of HMSFR masers. As shown in Figure 1(a), the distribution of young

OCs (<30 Myr) resembles that of HMSFR masers or O stars, revealing the major spiral arm segments in the vicinity of the Sun, i.e., the Perseus Arm, the Local Arm and the Sagittarius-Carina Arm. Some OCs seem to reside in an arm spur which branches between the Local Arm and the Sagittarius Arm (Xu et al. 2016). For the medium-young clusters with ages from 30 to 100 Myr, their distribution deviates from the arm segments defined by recent star formation (Fig. 1b). A majority of them are located around the Local Arm, and quite a few OCs are in the inter-arm regions. Intermediate-aged (100–200 Myr) and old clusters (>200 Myr) are more loosely distributed in the Galactic region covering the three arm segments as featured in Figure 1(c) and Figure 1(d), and no obvious arm-like features are visible. These properties are in general consistent with previous results (e.g., Dias & Lépine 2005; Cantat-Gaudin et al. 2018).

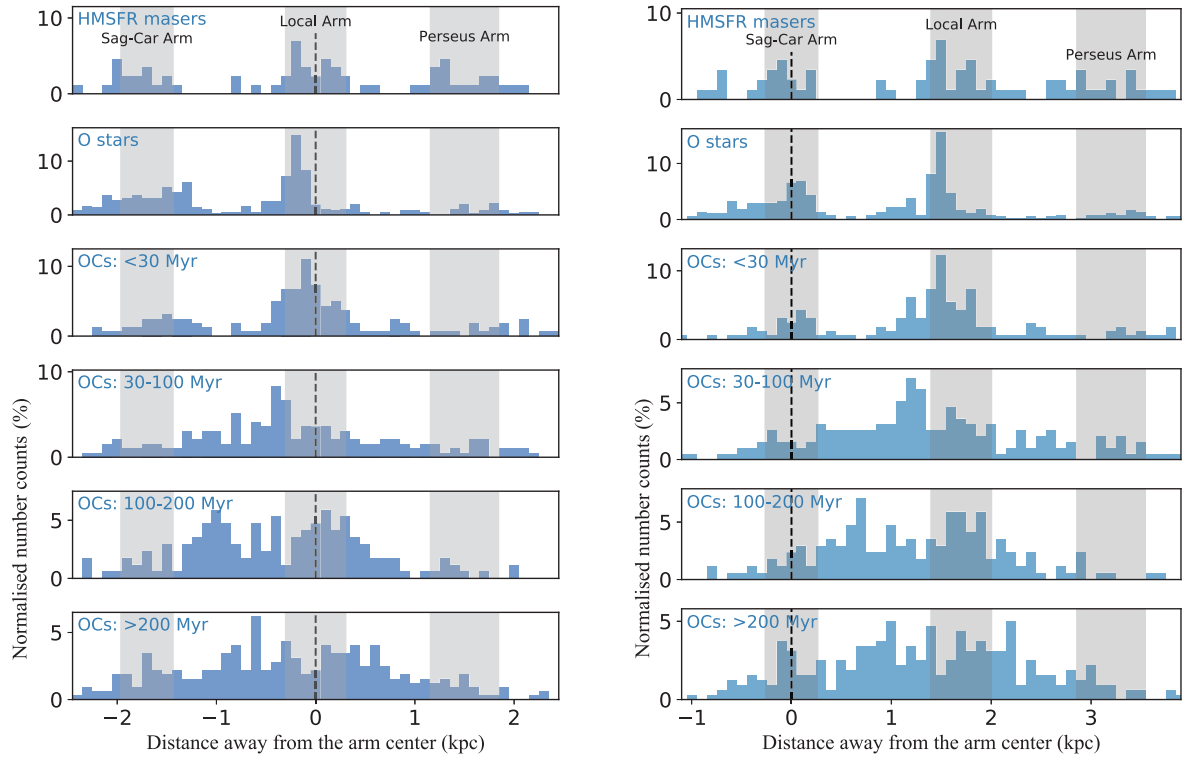


Fig. 2 Number counts of objects as a function of their distances away from the center of the Local Arm (*left*) and the Sagittarius-Carina Arm (*right*). Positive distances represent the outer side of the arm (i.e., to the GAC direction), and negative distances are towards the opposite side (i.e., to the GC direction). Each plot is normalised to the total number of the sample.

In order to clearly reveal the possible age pattern, we plot the number counts of objects as a function of their distances away from the center of a spiral arm. The arm positions fitted by Reid et al. (2019) are adopted in our calculations. As visible in Figure 2, from the distribution of HMSFR masers, we can find three bump features, which correspond to the Sagittarius-Carina Arm, the Local Arm and the Perseus Arm from left to right respectively. Similar bump features can be identified from the distributions of O stars and young OCs (<30 Myr), except the Perseus Arm, which is dim, probably due to the incompleteness of O stars and OCs in this Galaxy region at the moment. The peak positions of the bump features traced by HMSFR masers, O stars and young OCs seem to be not consistent with each other. For the young OCs in the Local Arm, they are distributed in broader regions than HMSFR masers or O stars. The bump peaks of young OCs and O stars are slightly inward (<100 pc) with respect to those of HMSFR masers (i.e., the vertical dashed lines). For the Sagittarius-Carina Arm, the bump peaks traced by O stars and young OCs slightly deviate outward (Galactic Anticenter (GAC) direction) with respect to the peak traced by HMSFR masers. The mean position offset is ~ 150 pc, roughly about half of the arm width (table 2 of Reid et al. 2019).

However, if considering the statistical error, the differences are not significant. In the distribution of the medium-young OCs (30–100 Myr), there is only one obvious bump, which is probably corresponding to the Local Arm (see the simulation results in Sect. 3.3). In this circumstance, the Local Arm traced by the medium-young clusters will clearly deviate inward with respect to the arms indicated by HMSFR masers, O stars or young OCs. In the distribution of the intermediate-aged (100–200 Myr) clusters, it seems that there are two bump features, one is near $x \sim -1$ kpc, the other is close to $x \sim 0.3$ kpc as displayed in the left panel of Figure 2. However, their correspondences to the star formation arms are not clear, as no obvious arm-like features are visible from their distributions (see Fig. 1). The old clusters (>200 Myr) are scattered widely, and no obvious bump features can be reliably identified.

In the longitude range of $\sim 240^\circ$ to 340° , there is a lack of HMSFR masers with accurate parallax measurements, which may influence the results given in Figure 2. Therefore, we divide each of the samples into two groups, one is for the 1st and 2nd Galactic quadrant regions ($0^\circ < l < 180^\circ$), the other is for the 3rd and 4th quadrants ($180^\circ < l < 360^\circ$), then replot the number counts of objects as a function of their distances away from the

centers of spiral arms. The results confirm the properties discussed above for the Sagittarius-Carina Arm and the Local Arm.

3.2 Kinematic Properties

Besides the age pattern, spiral density waves, if they exist, may also influence the kinematic properties of spiral tracers. With the radial velocities, parallaxes and proper motions from the *Gaia* DR2, we compare the kinematic properties of O stars and OCs. In the calculations, we adopt the solar motions with respect to the local standard of rest as $[U_\odot, V_\odot, W_\odot] = [10.6, 10.7, 7.6] \text{ km s}^{-1}$, the local circular velocity $\Theta_0 = 236 \text{ km s}^{-1}$, and the distance of the Sun to the GC $R_0 = 8.15 \text{ kpc}$ (Reid et al. 2019).

In Figure 3, we show the variation of circular velocity v_ϕ as a function of the Galactocentric radius R for the O stars and OCs of different age groups. As the Galactocentric radius increases, the overall circular velocity manifests a downward trend, which is consistent with that of the Galaxy rotation curve in the same range of Galactocentric radius (from about 6 kpc to 10.5 kpc, e.g., see Reid et al. 2019; Sofue 2020). As plotted in the right panels of Figure 3, the O stars tend to have smaller median v_ϕ and lag behind the young ($< 30 \text{ Myr}$) and medium-young clusters ($30\text{--}100 \text{ Myr}$) at $R \lesssim 8.2 \text{ kpc}$. While at $8.2 \lesssim R \lesssim 9.5 \text{ kpc}$, the O stars tend to have larger median v_ϕ and exceed the OCs. The typical uncertainty of v_ϕ is 0.9 km s^{-1} for OCs and 3.6 km s^{-1} for O stars, which indicate that the systematic velocity deviation between O stars and OCs is probably a true feature. In comparison to the younger clusters, the oldest OCs ($> 200 \text{ Myr}$) are distributed discretely, and may be dynamically relaxed. Linear fitting to the oldest OCs affirms that the circular velocity decreases by about $4.8 \text{ km s}^{-1} \text{ kpc}^{-1}$. In addition, their velocity distribution displays an interesting profile. The circular velocity oscillates and decreases along the Galactocentric radius, which suggests the v_ϕ of the oldest clusters tend to move systematically, which may be due to the perturbations of spiral arms (e.g., Liu et al. 2017).

The changes in radial motion v_r as a function of Galactocentric radius are given in Figure 4. The velocity distribution of the oldest clusters ($> 200 \text{ Myr}$) confirms that there is no obvious oscillation. However, in the inter-arm region between the Local Arm and the Sagittarius-Carina Arm, most of the old clusters have motions pointing to the GAC direction. While in the inter-arm region between the Local Arm and the Perseus Arm, a majority of the oldest clusters present an opposite situation, i.e., moving toward the GC direction. The median value of systematic motion is between 5 and 15 km s^{-1} .

3.3 Open Cluster Motions and Galaxy Spiral Arms

As demonstrated in Figure 2, there is a bump feature in the number counts of the medium-young OCs ($30\text{--}100 \text{ Myr}$) near $x \sim -0.4 \text{ kpc}$ (left panel). We speculate that it is probably related to the stellar Local Arm (Fig. 1). To verify this, we simulate the motions of OCs by means of their kinematic data.

We adopt a simplified model of the Galaxy proposed by Wu et al. (2009), which includes a Plummer potential bulge (Plummer 1911), an axisymmetric Galactic disc gravitational potential model (Allen & Santillan 1991; Miyamoto & Nagai 1975), and a logarithmic dark halo model. The Galaxy spiral potential may also influence the dynamics of OCs. However, the Galaxy spiral structure and hence the spiral potential have not been well modeled based on observations, and the effect of spiral potential is not considered in this simplified model. In addition, as the trace back time in this work is about tens of millions of years, quite smaller than the time of one Galactic rotation (a few hundred Myr), the influence of spiral potential on the OC dynamics is expected to be small. With the kinematic data (parallaxes, proper motions and radial velocities) of OCs and the Galactic gravitational potential model, we calculate the orbits of the medium-young OCs ($30\text{--}100 \text{ Myr}$), which are traced back to 30 Myr ago. As shown in Figure 5, a majority of the OCs are traced back to the GAC direction, and concentrated near the Galactic radius of $\sim 8 \text{ kpc}$, probably associated with the Local Arm at that time. In order to verify this, we assume that the spiral pattern of the Milky Way is stable within 30 Myr and rotate it back to 30 Myr ago by using a constant pattern speed. The assumption of a rigidly rotating spiral pattern is not realistic for all kinds of spiral galaxies, but for the Milky Way, it may be reasonable as some indications have been discussed (e.g., see Dias & Lépine 2005; Dias et al. 2019). With the pattern speed $\Omega_p = 28.2 \pm 2.1 \text{ km s}^{-1} \text{ kpc}^{-1}$ suggested by Dias et al. (2019), the nearby spiral pattern is rotated back to 30 Myr ago and compared with the distribution of OCs at that time. In this circumstance, we found that a majority of the medium-young OCs ($30\text{--}100 \text{ Myr}$) in the bump feature are moved $\sim 400 \text{ pc}$ toward the GAC direction, and traced back to the Local Arm (right panel of Fig. 5). The results are consistent with our speculation that the bump feature present in the distribution of the medium-young OCs ($30\text{--}100 \text{ Myr}$) is related to the stellar Local Arm.

4 DISCUSSIONS AND CONCLUSIONS

With the most updated sample of Galactic HMSFR masers, O stars and OCs having parallax distances, proper motions and radial velocities, we compared their distributions and kinematic properties, aiming to better understand the properties of Galactic spiral arms. We found that the

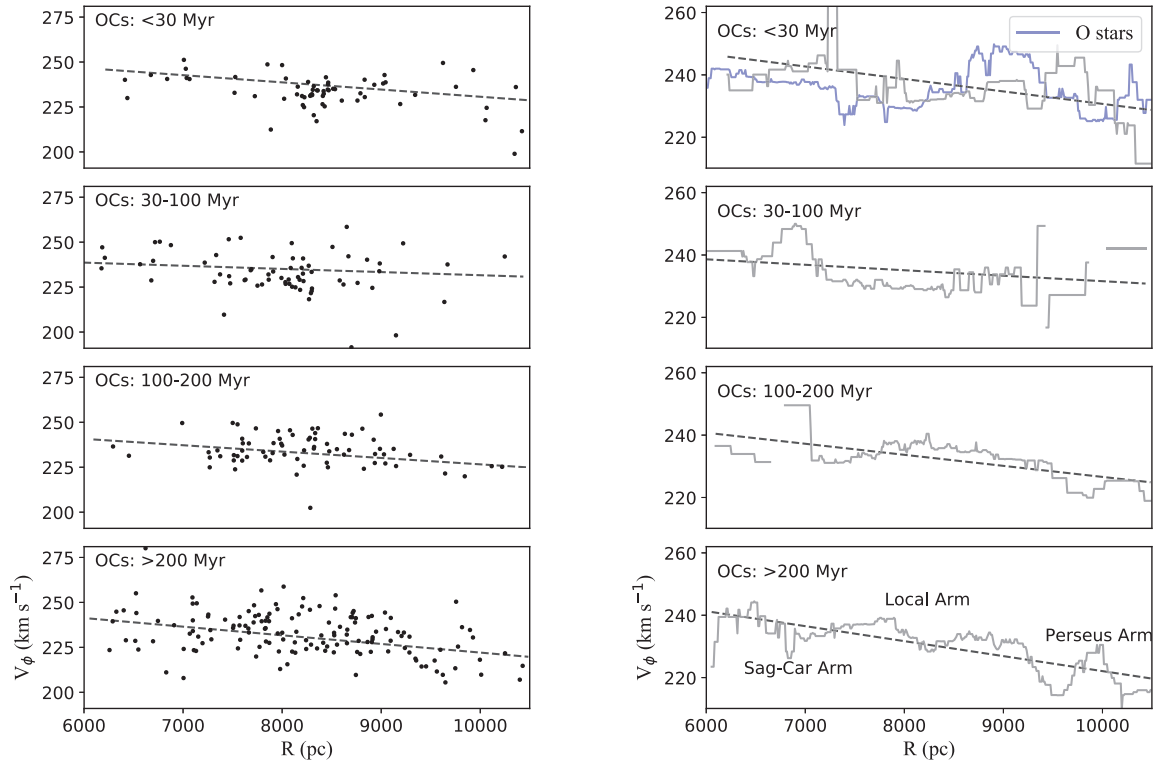


Fig. 3 *Left:* circular velocity v_ϕ as a function of Galactocentric radius R for the OCs of different age groups. *Right:* similar to the left panels, but the median values (bin size = 400 pc) are calculated and depicted as histograms for the OCs (gray solid lines). Also plotted are the results for the O stars (blue solid lines). In each panel, the black dashed line indicates a best linear fitting to the data of OCs. The median uncertainties σ_{v_ϕ} for O stars and OCs are 3.6 and 0.9 km s $^{-1}$, respectively.

Table 1 Published estimations of corotation radius R_c since 2000 in the form of R_c/R_0 . The values of R_0 are not the same in different references.

R_c/R_0	Method	References
0.83 ± 0.05^a	Measuring amplitude differential between stars and dust	Sect. 4.2 in Drimmel & Spergel (2001)
1.06 ± 0.08	Tracing back to the birthplace of star clusters	Sect. 4 in Dias & Lépine (2005)
1.11 ± 0.11	Gap in the radial HI density distribution	Sect. 3 in Amôres et al. (2009)
~ 0.89	Radial distribution of heavy elements	Sect. 4 in Acharova et al. (2012)
1.03^b	Stellar dynamics in the solar neighbourhood	Michtchenko et al. (2017)
1.07^c	Stellar dynamics in the solar neighbourhood	Michtchenko et al. (2018)
1.02 ± 0.07	Tracing back to the birthplace of <i>Gaia</i> DR2 star clusters	Sect. 6 in Dias et al. (2019)
1.01 ± 0.06^d	Offset traced by OCs	This work

[a] Pattern speed $\Omega_p = 25$ km s $^{-1}$ kpc $^{-1}$; [b] $\Omega_p = 26$ km s $^{-1}$ kpc $^{-1}$ from [Gerhard \(2011\)](#); [c] $\Omega_p = 28$ km s $^{-1}$ kpc $^{-1}$ from [Dias & Lépine \(2005\)](#); [d] $\Omega_p = 28.2 \pm 2.1$ km s $^{-1}$ kpc $^{-1}$ from [Dias et al. \(2019\)](#).

Sagittarius-Carina Arm traced by HMSFR masers, O stars ($\lesssim 10$ Myr) and young OCs (< 30 Myr) tends to gradually deviate toward the GAC direction. The Local Arm traced by HMSFR masers, O stars ($\lesssim 10$ Myr), young OCs (< 30 Myr) and medium-young clusters (30–100 Myr) is inclined to gradually deviate toward the GC direction. Especially for the medium-young OCs in the Local Arm, the deviation between its bump peak and those of the masers, O stars and young OCs is obvious. The properties of the Local Arm are also supported by a simplified simulation of the cluster motions. For the intermediate-

aged (100–200 Myr) or old clusters (> 200 Myr), their distributions do not exhibit any sign of age pattern, as they are distributed in a wide region covering the nearby three arm segments, and no obvious arm-like features can be identified. In the inner Galaxy regions near the tangency points of the Scutum–Centaurus Arm and maybe the Sagittarius Arm, [Hou & Han \(2015\)](#) also found that the old stellar arms deviate obviously from the gaseous/star-forming arms toward the GAC direction. These results jointly indicate that the deviations between old stellar and

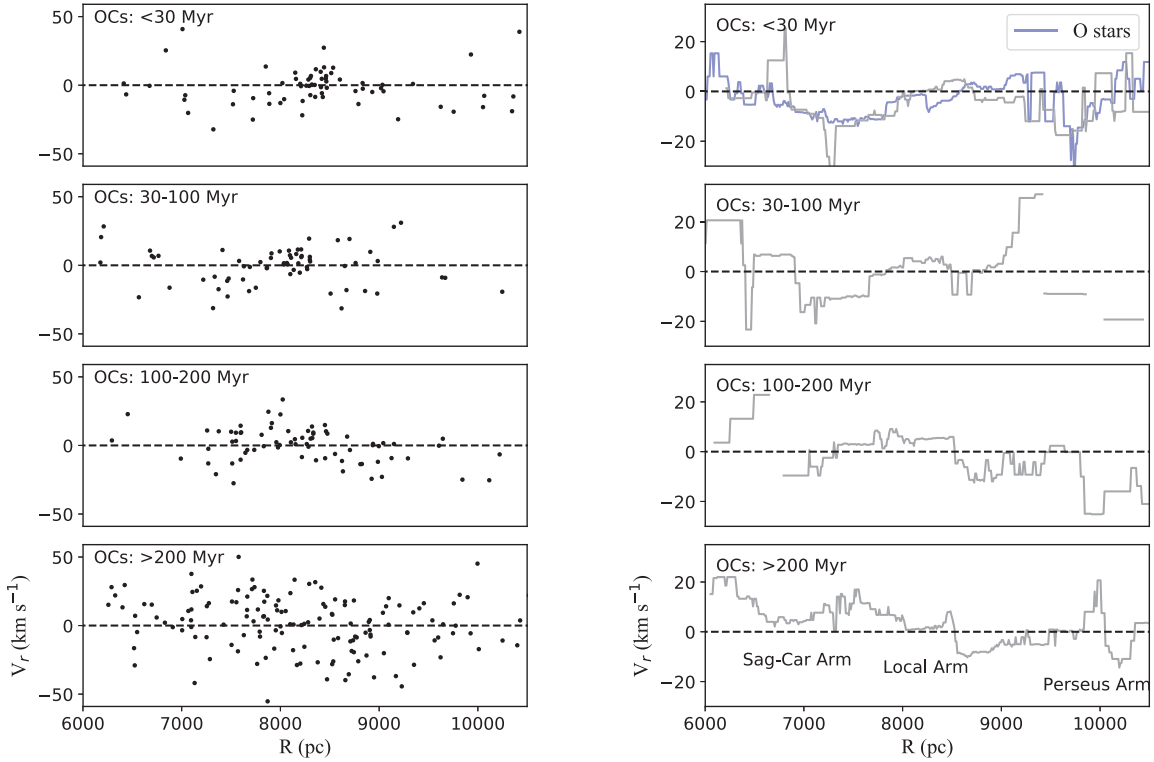


Fig. 4 Similar to Fig. 3, but for the radial velocity v_r . The median values of uncertainty σ_{v_r} for O stars and OCs are 1.0 and 0.8 km s^{-1} , respectively.

gaseous arms are probably not local features, but may be widespread in the Galaxy.

The results presented in this work are consistent with, as stated in Martínez-García et al. (2009), the notion that star formation can be triggered by spiral shocks of density waves. Among the leading ideas for the spiral arm formation (e.g., Wada et al. 2011; Baba et al. 2015; Dobbs & Pringle 2010), the density wave theory adopts a constant pattern speed, and hence predicts that the spiral shock (traced by star formation) will lie on one side of the stellar potential minimum within the corotation radius, and on the opposite side while outside the corotation radius (Dobbs & Baba 2014). In the star formation scenario, an age pattern from young to old (or a colour gradient from blue to red) along spiral arms is expected as a result of the stellar evolution. (Martínez-García et al. 2009; Dobbs & Pringle 2010; Shu 2016). A clear age pattern across spiral arms has been found in some grand-design spiral galaxies, e.g., UGC 3825 (Peterken et al. 2019) and NGC 1566 (Shabani et al. 2018).

Our results also suggest that the segment of the Sagittarius-Carina Arm in the vicinity of the Sun is probably still within the corotation radius R_c of the Galaxy. However, the Local Arm is already outside R_c . With the pattern speed $\Omega_p = 28.2 \pm 2.1 \text{ km s}^{-1} \text{ kpc}^{-1}$ obtained by Dias et al. (2019), we calculate the corotation

radius R_c by utilizing the median circular velocity v_ϕ of the old clusters (Sect. 3.2). The value of R_c is estimated to be at 7.69–8.74 kpc, corresponding to $R_c/R_0 = 1.01 \pm 0.06$ if $R_0 = 8.15 \text{ kpc}$ (Reid et al. 2019) is adopted. The result is compared with previous measurements as given in Table 1. Our inferences are consistent with some measurements of the corotation radius by applying different methods, which suggested that the corotation radius is outside the Sagittarius-Carina Arm, but close to the Solar circle (e.g., Drimmel & Spergel 2001; Acharova et al. 2012; Michtchenko et al. 2017; Dias et al. 2019).

In addition, spiral arms may cause streaming motions of gaseous or stellar components (also named peculiar motion, streaming velocity, etc.) beyond the pure circular rotations. For example, the density wave theory suggests that the radial velocities are largest at potential minima and maxima, whereas the circular velocities are largest at the inside and outside edges of spiral arms (Yuan 1969; Shu 2016). We noticed that the circular velocity (v_ϕ) of oldest OCs oscillates and decreases along the Galactocentric radius, which may be caused by spiral arms. In the plots of radial velocity, both the O stars and OCs show indications of systematic motions near the Sagittarius-Carina Arm, the Local Arm and the Perseus Arm. The systematic motion is between 5 and 15 km s^{-1} . It is comparable to

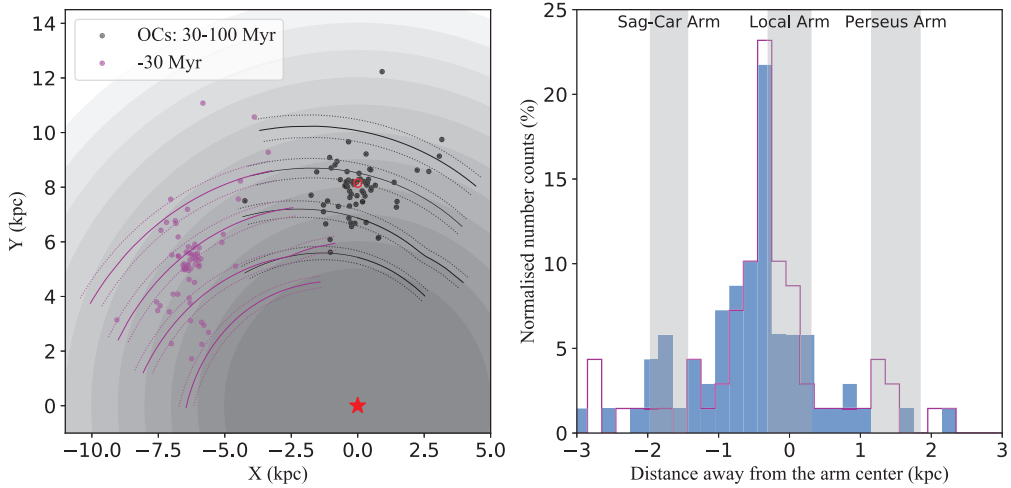


Fig. 5 *Left:* Distributions of medium-young OCs at present-day (*filled black circles*) and 30 Myr ago (*filled magenta circles*). The red star represents the position of the GC. The Sun (\odot) is at (0, 8.15) kpc. The direction of disk rotation is clockwise as viewed from the North Galactic Pole. The shaded portions of the Galactic plane represent different radii, starting at Galactocentric distance of 5 kpc and spaced with 1 kpc. Also plotted are the spiral arms at present-day (*black*) and 30 Myr ago (*magenta*) derived by assuming a rigidly rotating spiral pattern for the Milky Way. *Right:* Number counts of OCs as a function of their distances away from the center of the Local Arm ($x = 0$ kpc). The *filled histogram* (blue) and the *magenta coloured histogram* represent the OCs at present-day and 30 Myr ago, respectively.

the simulations of the axisymmetric features in kinematic spaces for different disc models with spiral structure by Antoja et al. (2016). They found that the typical velocity asymmetries were of the order of 2 to 10 km s^{-1} .

The results reported in this work give some clues for understanding the underlying dynamics of the Milky Way. However, the sample size of spiral tracers with accurate measurements of parallaxes, proper motions and radial velocities is still small, which limits the study to the nearby segments of the Local Arm and the Sagittarius-Carina Arm. In particular, the Sagittarius-Carina Arm traced by medium-young OCs (30–100 Myr) cannot be reliably identified with the available dataset. Recently, Miyachi et al. (2019) identified a stellar overdensity in the Local Arm, whose pitch angle is slightly larger than that of the Local Arm traced by HMSFRs. Their results pose questions to both the density wave theory and the dynamic spiral arm model. More observational tests are necessary. *Gaia* DR3 will be released soon, which will help to enlarge the sample of Galactic O stars and OCs, and also significantly improve the measurement accuracy of parallaxes, proper motions and radial velocities. With the *Gaia* DR3, we expect to inspect the possible age pattern for the nearby and also more distant spiral arm segments, in order to better understand the dynamic nature of Galactic spiral arms.

Acknowledgements We thank the anonymous referee for helpful comments and suggestions that improved this work. The authors thank Professor Tristan Cantat-

Gaudin for kindly providing us the latest cluster data and professor Mark J. Reid for guiding and checking the spiral arm figure we duplicated. This work has made use of data from the European Space Agency (ESA) mission *Gaia* (<https://www.cosmos.esa.int/Gaia>), processed by the *Gaia* Data Processing and Analysis Consortium (DPAC, <https://www.cosmos.esa.int/web/Gaia/dpac/consortium>). Funding for the DPAC has been provided by national institutions, in particular the institutions participating in the *Gaia* Multilateral Agreement. This work is supported by the National Key Research and Development Program of China (No. 2017YFA0402701) and the National Natural Science Foundation of China (Grant Nos. 11988101, 11933011, 11833009). LGH acknowledges support from the Youth Innovation Promotion Association, CAS.

References

- Acharova, I. A., Mishurov, Y. N., & Kovtyukh, V. V. 2012, *MNRAS*, **420**, 1590
- Allen, C., & Santillan, A. 1991, *RMxAA*, **22**, 255
- Amôres, E. B., Lépine, J. R. D., & Mishurov, Y. N. 2009, *MNRAS*, **400**, 1768
- Ann, H. B., Seo, M., & Ha, D. K. 2015, *ApJS*, **217**, 27
- Antoja, T., Roca-Fàbrega, S., de Bruijne, J., & Prusti, T. 2016, *A&A*, **589**, A13
- Athanassoula, E., Romero-Gómez, M., Bosma, A., & Masdemont, J. J. 2010, *MNRAS*, **407**, 1433
- Baba, J., Asaki, Y., Makino, J., et al. 2009, *ApJ*, **706**, 471

- Baba, J., Saitoh, T. R., & Wada, K. 2010, PASJ, 62, 1413
- Baba, J., Morokuma-Matsui, K., & Egusa, F. 2015, [PASJ, 67, L4](#)
- Bovy, J., Bird, J. C., García Pérez, A. E., et al. 2015, [ApJ, 800, 83](#)
- Cantat-Gaudin, T., & Anders, F. 2020, [A&A, 633, A99](#)
- Cantat-Gaudin, T., et al. 2018, [A&A, 618, A93](#)
- Cantat-Gaudin, T., et al. 2019, [A&A, 624, A126](#)
- Cantat-Gaudin, T., et al. 2020, arXiv e-prints, p. [arXiv:2004.07274](#)
- Castro-Ginard, A., Jordi, C., Luri, X., et al. 2018, [A&A, 618, A59](#)
- Castro-Ginard, A., Jordi, C., Luri, X., Cantat-Gaudin, T., & Balaguer-Núñez, L. 2019, [A&A, 627, A35](#)
- Castro-Ginard, A., et al. 2020, [A&A, 635, A45](#)
- Chandar, R., et al. 2017, [ApJ, 845, 78](#)
- Chen, B. Q., et al. 2019, [MNRAS, 487, 1400](#)
- Cheng, X., Liu, C., Mao, S., & Cui, W. 2019, [ApJL, 872, L1](#)
- Dias, W. S., & Lépine, J. R. D. 2005, [ApJ, 629, 825](#)
- Dias, W. S., Alessi, B. S., Moitinho, A., & Lépine, J. R. D. 2002, [A&A, 389, 871](#)
- Dias, W. S., Monteiro, H., Lépine, J. R. D., & Barros, D. A. 2019, [MNRAS, 486, 5726](#)
- Dobbs, C., & Baba, J. 2014, [PASA, 31, e035](#)
- Dobbs, C. L., & Pringle, J. E. 2010, [MNRAS, 409, 396](#)
- Dobbs, C. L., Theis, C., Pringle, J. E., & Bate, M. R. 2010, [MNRAS, 403, 625](#)
- Drimmel, R., & Spergel, D. N. 2001, [ApJ, 556, 181](#)
- Faure, C., Siebert, A., & Famaey, B. 2014, [MNRAS, 440, 2564](#)
- Gaia Collaboration, et al. 2016, [A&A, 595, A1](#)
- Gaia Collaboration, et al. 2018, [A&A, 616, A1](#)
- Georgelin, Y. M., & Georgelin, Y. P. 1976, [A&A, 49, 57](#)
- Gerhard, O. 2011, Memorie della Societa Astronomica Italiana Supplementi, [18, 185](#)
- Goldreich, P., & Tremaine, S. 1978, [ApJ, 222, 850](#)
- Gómez, F. A., Minchev, I., et al. 2013, [MNRAS, 429, 159](#)
- Grand, R. J. J., Kawata, D., & Cropper, M. 2012, [MNRAS, 421, 1529](#)
- Griv, E., Gedalin, M., Shih, I. C., et al. 2020, [MNRAS, 493, 2111](#)
- Hart, R. E., Bamford, S. P., Hayes, W. B., et al. 2017, [MNRAS, 472, 2263](#)
- Hou, L. G., & Han, J. L. 2014, [A&A, 569, A125](#)
- Hou, L. G., & Han, J. L. 2015, [MNRAS, 454, 626](#)
- Hunt, J. A. S., Kawata, D., Monari, G., et al. 2017, [MNRAS, 467, L21](#)
- Kawata, D., Baba, J., Ciucă, I., et al. 2018, [MNRAS, 479, L108](#)
- Kharchenko, N. V., Piskunov, A. E., Schilbach, E., Röser, S., & Scholz, R. D. 2013, [A&A, 558, A53](#)
- Kuminski, E., & Shamir, L. 2016, [ApJS, 223, 20](#)
- Levine, E. S., Blitz, L., & Heiles, C. 2006, [Science, 312, 1773](#)
- Lin, C. C., & Shu, F. H. 1964, [ApJ, 140, 646](#)
- Lin, C. C., & Shu, F. H. 1966, Proceedings of the National Academy of Science, 55, 229
- Lindblad, B. 1963, Stockholms Observatoriums Annaler, [5, 5](#)
- Lindegren, L., et al. 2018, [A&A, 616, A2](#)
- Liu, L., & Pang, X. 2019, [ApJS, 245, 32](#)
- Liu, C., et al. 2017, [ApJL, 835, L18](#)
- Martínez-García, E. E., González-Lópezlira, R. A., & Bruzual-A, G. 2009, [ApJ, 694, 512](#)
- Masters, K. L., et al. 2019, [MNRAS, 487, 1808](#)
- Michtchenko, T. A., Vieira, R. S. S., Barros, D. A., & Lépine, J. R. D. 2017, [A&A, 597, A39](#)
- Michtchenko, T. A., Lépine, J. R. D., et al. 2018, [ApJL, 863, L37](#)
- Miller, R., Kennefick, D., et al. 2019, [ApJ, 874, 177](#)
- Miyachi, Y., Sakai, N., Kawata, D., et al. 2019, [ApJ, 882, 48](#)
- Miyamoto, M., & Nagai, R. 1975, [PASJ, 27, 533](#)
- Monguió, M., Grosbøl, P., & Figueras, F. 2015, [A&A, 577, A142](#)
- Peterken, T. G., Merrifield, M. R., et al. 2019, [Nature Astronomy, 3, 178](#)
- Plummer, H. C. 1911, [MNRAS, 71, 460](#)
- Pringle, J. E., & Dobbs, C. L. 2019, [MNRAS, 490, 1470](#)
- Puerari, I., & Dottori, H. 1997, [ApJL, 476, L73](#)
- Reed, B. C. 2003, [AJ, 125, 2531](#)
- Reid, M. J., et al. 2019, [ApJ, 885, 131](#)
- Roberts, W. W. 1969, [ApJ, 158, 123](#)
- Sanders, R. H., & Huntley, J. M. 1976, [ApJ, 209, 53](#)
- Sellwood, J. A., & Carlberg, R. G. 1984, [ApJ, 282, 61](#)
- Sellwood, J. A., & Sparke, L. S. 1988, [MNRAS, 231, 25P](#)
- Shabani, F., Grebel, E. K., Pasquali, A., et al. 2018, [MNRAS, 478, 3590](#)
- Shu, F. H. 2016, [ARA&A, 54, 667](#)
- Sofue, Y. 2020, arXiv e-prints, p. [arXiv:2004.11688](#)
- Soubiran, C., et al. 2018, [A&A, 619, A155](#)
- Tagger, M., Sygnet, J. F., Athanassoula, E., & Pellat, R. 1987, [ApJL, 318, L43](#)
- Toomre, A. 1981, in Fall S. M., Lynden-Bell D., eds, Structure and Evolution of Normal Galaxies. pp 111–136
- Toomre, A., & Toomre, J. 1972, [ApJ, 178, 623](#)
- Vallée, J. P. 2018, [ApJ, 863, 52](#)
- Wada, K., Baba, J., & Saitoh, T. R. 2011, [ApJ, 735, 1](#)
- Willett, K. W., et al. 2013, [MNRAS, 435, 2835](#)
- Williams, M. E. K., et al. 2013, [MNRAS, 436, 101](#)
- Wu, Z.-Y., Zhou, X., Ma, J., & Du, C.-H. 2009, [MNRAS, 399, 2146](#)
- Xu, Y., et al. 2016, [Science Advances, 2, e1600878](#)
- Xu, Y., Hou, L.-G., & Wu, Y.-W. 2018a, [RAA \(Research in Astronomy and Astrophysics\), 18, 146](#)
- Xu, Y., et al. 2018b, [A&A, 616, L15](#)
- Yu, S.-Y., & Ho, L. C. 2018, [ApJ, 869, 29](#)
- Yuan, C. 1969, [ApJ, 158, 871](#)